The Astrophysical Journal, 830:132 (8pp), 2016 October 20 doi:10.3847/0004-637X/830/2/132

RELATIONSHIP BETWEEN DISTRIBUTION OF MAGNETIC DECAY INDEX AND FILAMENT ERUPTIONS

H. Li[1,2], Y. Liu[1], A. Elmhamdi[3], and A.-S. Kordi[3]
[1] Yunnan Observatories, Chinese Academy of Sciences, Kunming 650011, China; hbli@ynao.ac.cn
[2] Graduate School of Chinese Academy of Science, Beijing 100049, China
[3] Department of Physics and Astronomy, King Saud University, P.O. Box 2455, 11451, Saudi Arabia
Received 2015 August 17; revised 2016 July 30; accepted 2016 August 4; published 2016 October 18

ABSTRACT

The decay index n of a horizontal magnetic field is considered to be an important parameter in judging the stability of a flux rope. However, the spatial distribution of this parameter has not been extensively explored so far. In this paper, we present a delineative study of the three-dimensional maps of n for two eruptive events, in which filaments underwent asymmetrical eruptions. The corresponding n-distributions are both found to show that the filaments tend to erupt at abnormal regions (dubbed ABN regions) of n. These ABN regions appear to be divided into two subregions, with larger and smaller n. Moreover, an analysis of the magnetic topological configuration of the ABN regions has been also performed. The results indicate that these ABN regions are associated with a kind of special quasi-separatrix layer across which the connectivity of magnetic field is discontinuous. The presented observations and analyses strongly suggest that the torus instability in ABN regions may play a crucial role for the triggering of an asymmetrical eruption. Additionally, our investigation can provide a way of forecasting how a filament might erupt, and predicting the location for an asymmetrically eruptive filament to be split through analyzing the spatial structure of n.

Key words: Sun: activity – Sun: filaments, prominences – Sun: magnetic fields

1. INTRODUCTION

Solar filaments, as some of the most common structures in the coronal atmosphere, are often observed suspended in the hot and tenuous solar atmosphere for a long period (usually a few days to a few weeks; Parenti 2014). In a stable situation, they are generally considered as dense and cool plasmas supported by the coronal magnetic field, and are also observational evidence of magnetic flux ropes extending into the corona. Most filaments also manifest in more dynamical processes, namely filament eruptions. These fierce phenomena, with their intimate connection with flares and coronal mass ejections (see Low 1996), have been extensively studied over the last two decades (Forbes 2000; Lin & Forbes 2000; Zhang 2002; Hudson et al. 2006). In these studies, three phenomena are suggested to originate from the same physical process, which involves the reconnection of the magnetic field and the release of magnetic energy (Forbes 2000; Priest & Forbes 2002).

Filaments can erupt in different ways, including symmetric and asymmetric eruption, distinguishable by whether they exhibit a symmetric form during the eruptions or not. Eruptive filaments often show an asymmetric process of eruption, in which the filament splits away from one leg, with the other leg remaining fixed to the photosphere (Tripathi et al. 2006; Liu et al. 2009a). These observational characteristics of asymmetric eruptive filaments make them suitable and relevant for testing the validity of the eruptive models and the corresponding triggering mechanisms (Liu et al. 2009b).

Concerning the triggering mechanisms of filament eruptions, both theoretical and numerical studies indicate kink and torus instabilities as two possible candidates (Török & Kliem 2005; Kliem & Török 2006; Fan & Gibson 2007). Beyond that, it is also suggested that the magnetic decay index n (Bateman 1978), a gradient of the horizontal magnetic field decreasing versus the height, is crucial to ascertain whether the background magnetic field is vulnerable to a torus instability and whether a kink instability might develop into a filament eruption. According to the analyses of Bateman (1978) and Kliem & Török (2006), a critical index may be between 1.5 and 2, so we will take the middle value, i.e., 1.75, as the critical index in the present study. Observationally, many studies also indicate that n can be used to estimate the probability of the occurrence of a filament eruption (Liu 2008; Filippov et al. 2014). Recently, Zuccarello et al. (2014) reported an eruption initiated when the filament reached a critical height where the decay index had a larger value. However, the spatial distribution of this parameter has never been given adequate attention. Evidently, the spatial distribution of n is inhomogeneous because of the complex structure of the coronal magnetic field, which most likely has some influence on filament eruptions, especially the asymmetric ones.

In this paper, we investigate two asymmetric filament eruptions and carefully examine the spatial distribution of the decay index n over them. In order to have a clear understanding of the relationship between the spatial distribution of n and the studied filament eruptions, the topological configuration of the magnetic field has also been explored, and a model is proposed for this type of eruptive event. Our data and method are shown in the next section. The analysis is given in Section 3. Finally, a discussion and conclusions are presented in Section 4.

2. OBSERVATIONS

In order to probe the eruptive processes of filaments, we exploit images from the Atmospheric Imaging Assembly (AIA; Lemen et al. 2012) on board the *Solar Dynamics Observatory* (*SDO*; Pesnell et al. 2012). The AIA observations are taken at 12 s temporal cadence with a spatial resolution of $0\farcs6$. In addition, images from the Extreme Ultraviolet Imager (EUVI; Wuelser et al. 2004) on board the twin *Solar Terrestrial Relations Observatory* (*STEREO*; Kaiser et al. 2008) spacecraft

Table 1
Details of the Two Filament Eruption Events

No.	Data	Start (UT)	End (UT)	Location	NOAA	Flare	Feature
1	2011 May 02	13:10	16:10	S22E39	⋯	⋯	Partially broken
2	2011 Jun 05	02:06	06:06	N32E34	11231	⋯	Partially broken

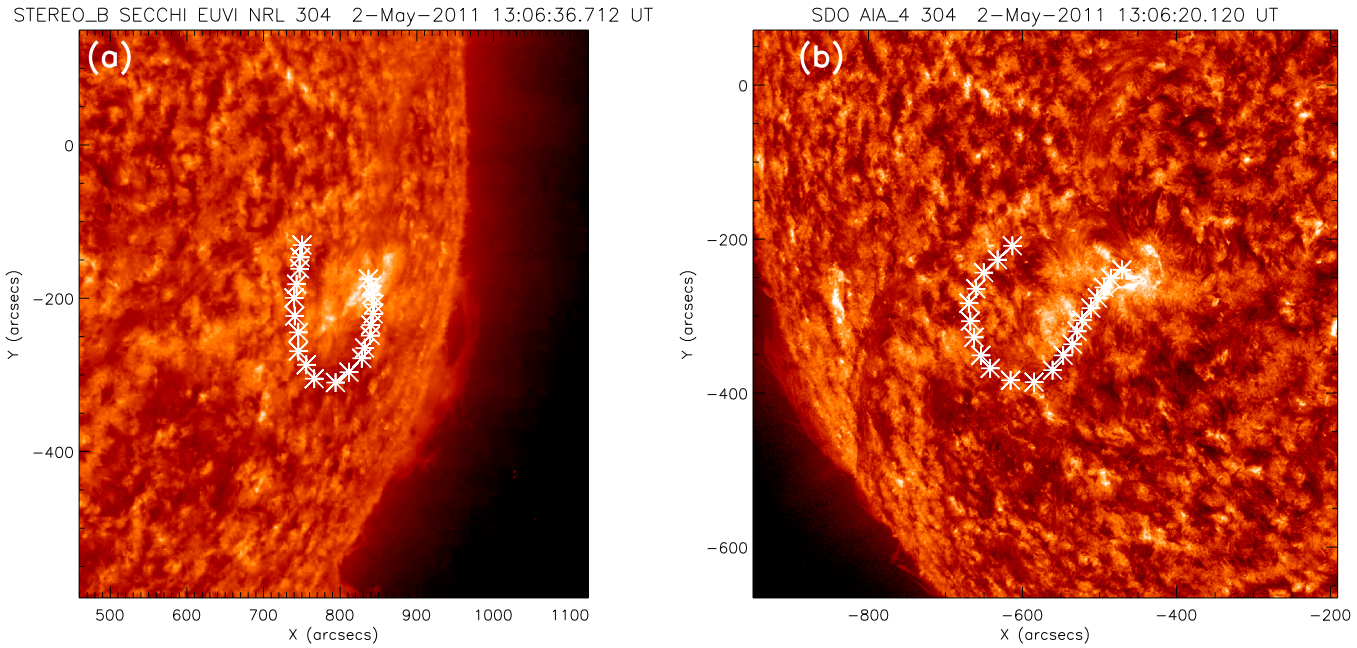

Figure 1. An overview of F1 observed by the AIA at 304 Å (a) and EUVI-B at 304 Å (b) on 2011 May 2. F1 is marked as a series of asterisk on both images.

(henceforth *STEREO_A* and *STEREO_B*) are necessary for calculating the three-dimensional coordinates of the filaments. The EUVI images are supplied with a time cadence of 5/10 minutes in the 195/304 Å channel and their pixel size is 1.″6.

For the purpose of calculating the decay index n, we use the global Potential Field Source Surface model (PFSS; Schrijver & De Rosa 2003) as the coronal magnetic field over the photosphere, computed from a full-sphere synoptic map of the evolving photospheric field, based on assimilated *Solar and Heliospheric Observatory* (*SOHO*)/MDI (Scherrer et al. 1995) magnetograms. In our study, this model is justified, since our research regions are on a large scale and the magnetic sources of those regions are not isolated from other sources, all of which match with a large-scale and spherical magnetic model. Moreover, the selected events are all within 60° form the disk center, where the real time *SOHO*/MDI data are assimilated as the input data for the PFSS model. Additionally, our main concern is the instability of the overlying field of filaments and its relevance to filament eruptions, which is in accordance with the potential field approximation.

3. ANALYSIS

3.1. Filament Eruption No. 1

The filament in event 1 (F1) was observed near the disk center by the *SDO* on 2011 May 2 (Table 1). An overview of F1 is shown in Figure 1 from both *SDO* and *STEREO_B* views. The sequential progress of the eruption is illustrated in Figure 2. F1's body is overplotted (asterisk-symbol lines) on the images. The location where F1 was broken is marked by a white arrow in Figure 2(b). The process of the eruption started at about 13:10 UT. Over the next three hours, F1 was observed to gradually expand and then rapidly run away from its eastern foot-point. During the eruption, the rest of F1 remained fixed on its western foot-point and ejected along a loop-like trajectory instead of moving out symmetrically. All these performances indicate that F1 underwent a typical asymmetric eruption (Tripathi et al. 2006) and there should be some asymmetric factors accounting for the apparent split of F1's eastern leg.

Next, we calculated the decay index n of the horizontal magnetic field over F1. According to Bateman (1978), n is defined as follows:

$$n = \frac{d \log B_{\rm h}}{d \log H}, \quad (1)$$

with $B_{\rm h}$ is the horizontal component of the external magnetic field, and H refers to the height. It is noteworthy that there would be some particular cases in the computation, notably for points with $B_{\rm h} = 0$. Indeed, these particular points can cause a diverging n (i.e., tending to infinity). However, this will not have a significant impact in our present investigation, since we have inspected all possibilities for $B_{\rm h}$ that we are interested in,

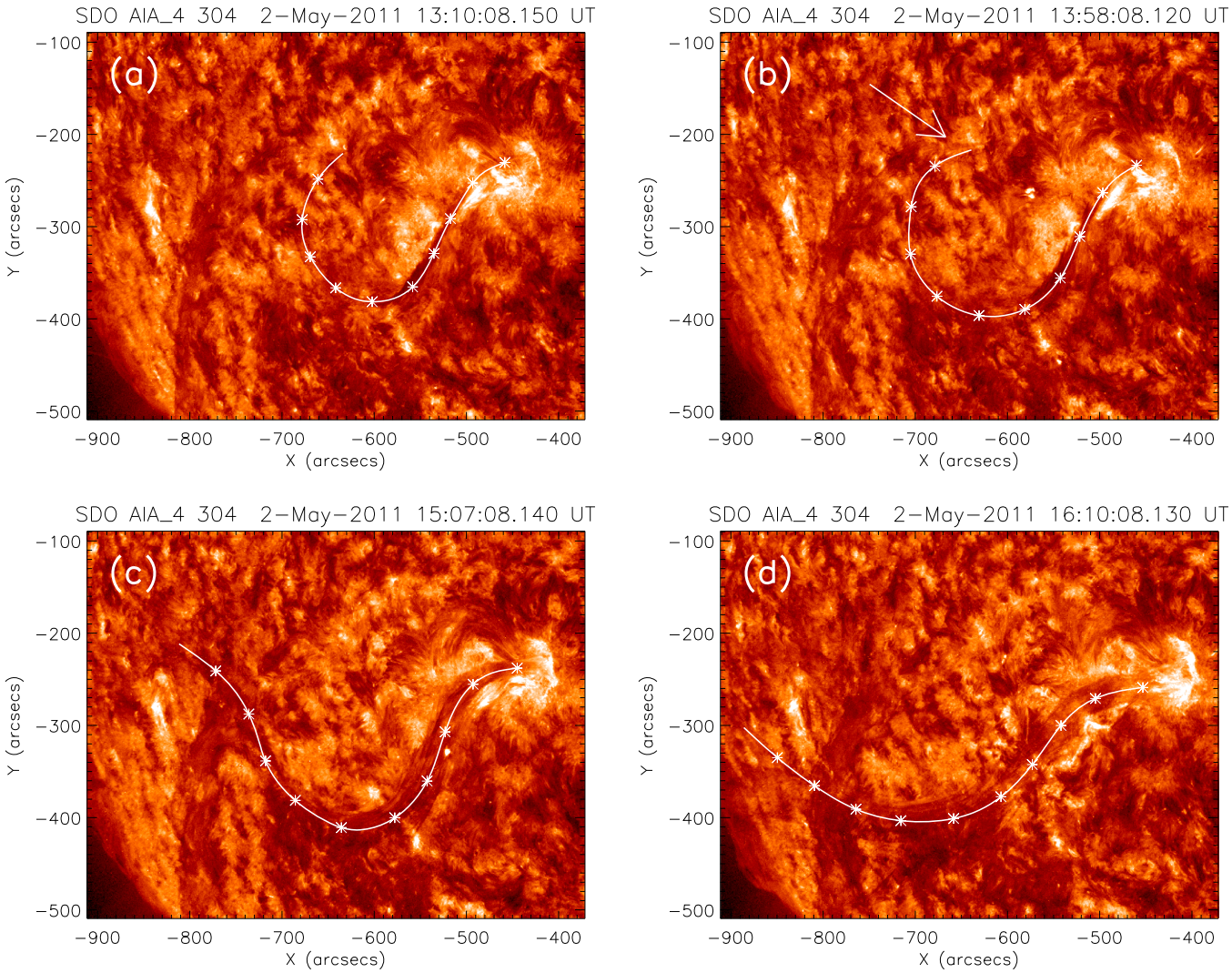

Figure 2. The evolution and eruption of F1 shown by AIA 304 Å images. The bodies of F1 are indicated by the white asterisk lines. The white arrow in frame (b) shows the fractured location of F1.

and have found no particular point where the horizontal magnetic field vanishes. Moreover, these peculiar situations are rare in the PFSS model; hence we can neglect them in our analysis.

In order to provide a overall view of the distribution of the index n, a three-dimensional map is constructed. In this map, we plot n and overlap the filament on the radial transection along filament's projection line. As can be seen in Figure 3(a), the map of n (n-map) can be obtained along the filament's shadow line on the photosphere. In the n-maps, displayed in Figure 4, we find that an abnormal region of n (hereafter the ABN region) consisting of two combined subregions, one with larger n and the other with smaller n, is located near the split leg of F1 at 13:06 UT. Then, a gradual rise brought the eastern end of F1 into the lower subregion of this ABN region at around 13:46 UT. At the same time, the F1 started to split away from its eastern leg and an evident disconnection can be seen. The lower subregion of the ABN region is identified as the dotted contour in Figure 4, in which n exceeds the critical value of 1.75. A three-dimensional representative view of F1 and n is shown in Figure 3(c). These observations strongly suggest that there exists a close relationship between the asymmetric eruption of F1 and the distribution of the corresponding n-index over it.

3.2. Filament Eruption No. 2

Adopting the same approach used in the analysis of event 1, we studied the second event reported in Table 1. The filament (F2) in event 2 is located on the verge of the NOAA active region 11231, with an eruption starting at 02:06 UT. The evolution of the F2 is shown in Figure 5. In this event, F2 also underwent an asymmetric eruption. During the process of eruption, F2's southern leg was still anchored into the photosphere, while its other leg underwent a fierce dynamic motion and an accelerated cut-off from the surface of the Sun. This behavior indicates F2 also underwent an asymmetric eruption, which was very similar to the eruption of F1. Intriguingly, we also find an ABN region in the n-maps of F2 and it appears definitely adjacent to the eruptive leg of F2 (see Figure 6). The correspondence between the ABN region and the active leg of F2, and the split of F2's northern leg, provide us with further evidence for the torus instability in ABN

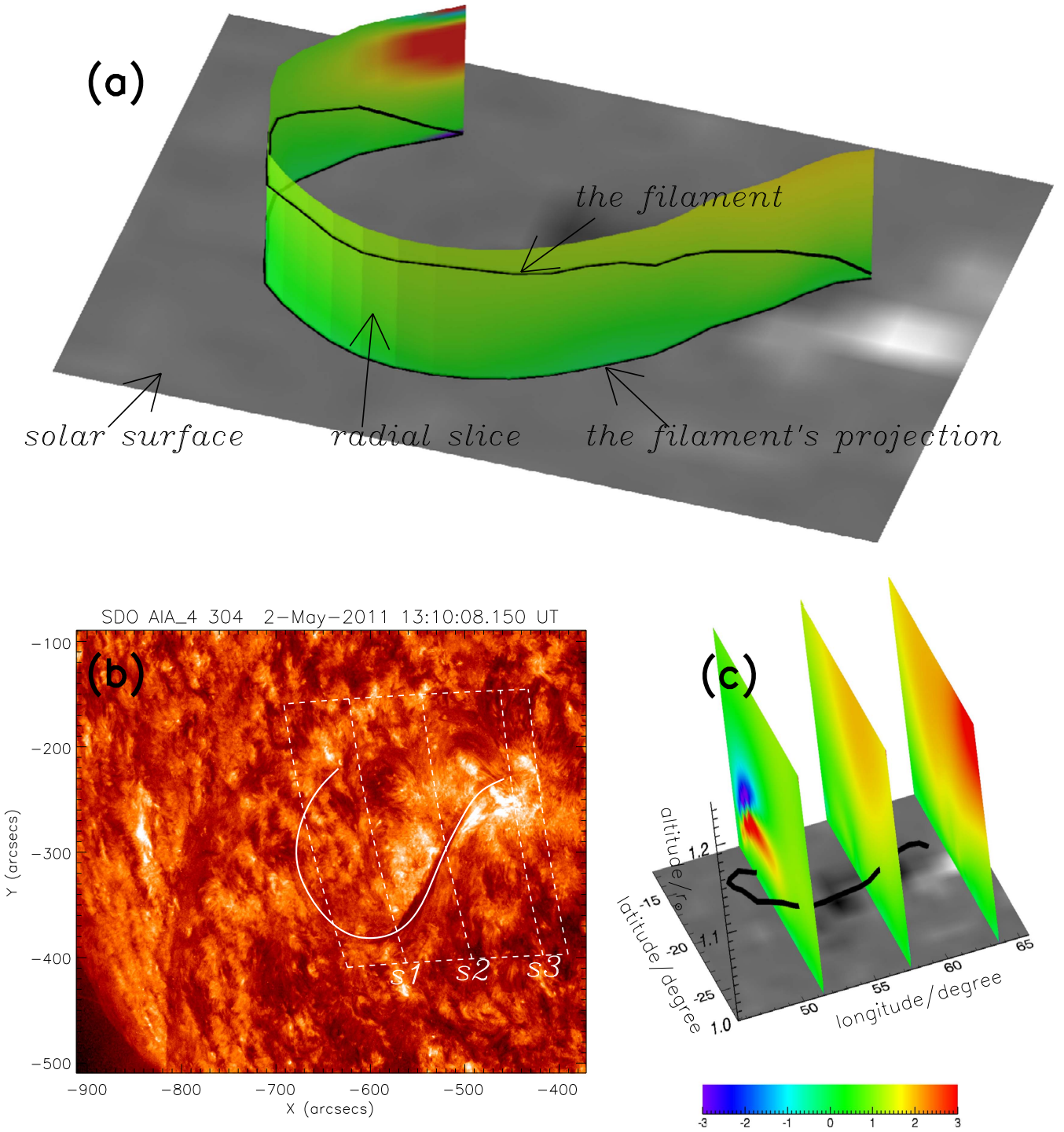

Figure 3. Schematic diagram demonstrating how we obtain the decay index n slice. The solar surface, decay index slice, three-dimension position of F1, and its shadow line are all marked on frame (a). The decay index n is shown in the planes overlapping on the magnetogram at the active region. The box of the magnetogram shown in panel (c) is indicated by the white dashed box in panel (b). The three lines s1, s2, s3 in panel (b) indicate the projections of the three planes for displaying n. The white solid curve line in panel (b) indicates the body of F1.

regions being the most likely triggering mechanism behind the rupture of the filament's body in an asymmetric eruption.

4. DISCUSSION AND CONCLUSIONS

The gradient of the horizontal potential field with respect to height, known as the decay index n, is suggested to be a significant parameter in deciding whether a filament eruption evolves to a successful full eruption or to a failed one (Török & Kliem 2005; Kliem & Török 2006; Filippov et al. 2014). Actually, the decay index n over a real filament is similar to the overlying magnetic field, which often has a complex distribution in space. Does this complex distribution of n have an impact on the filaments' eruption? To answer

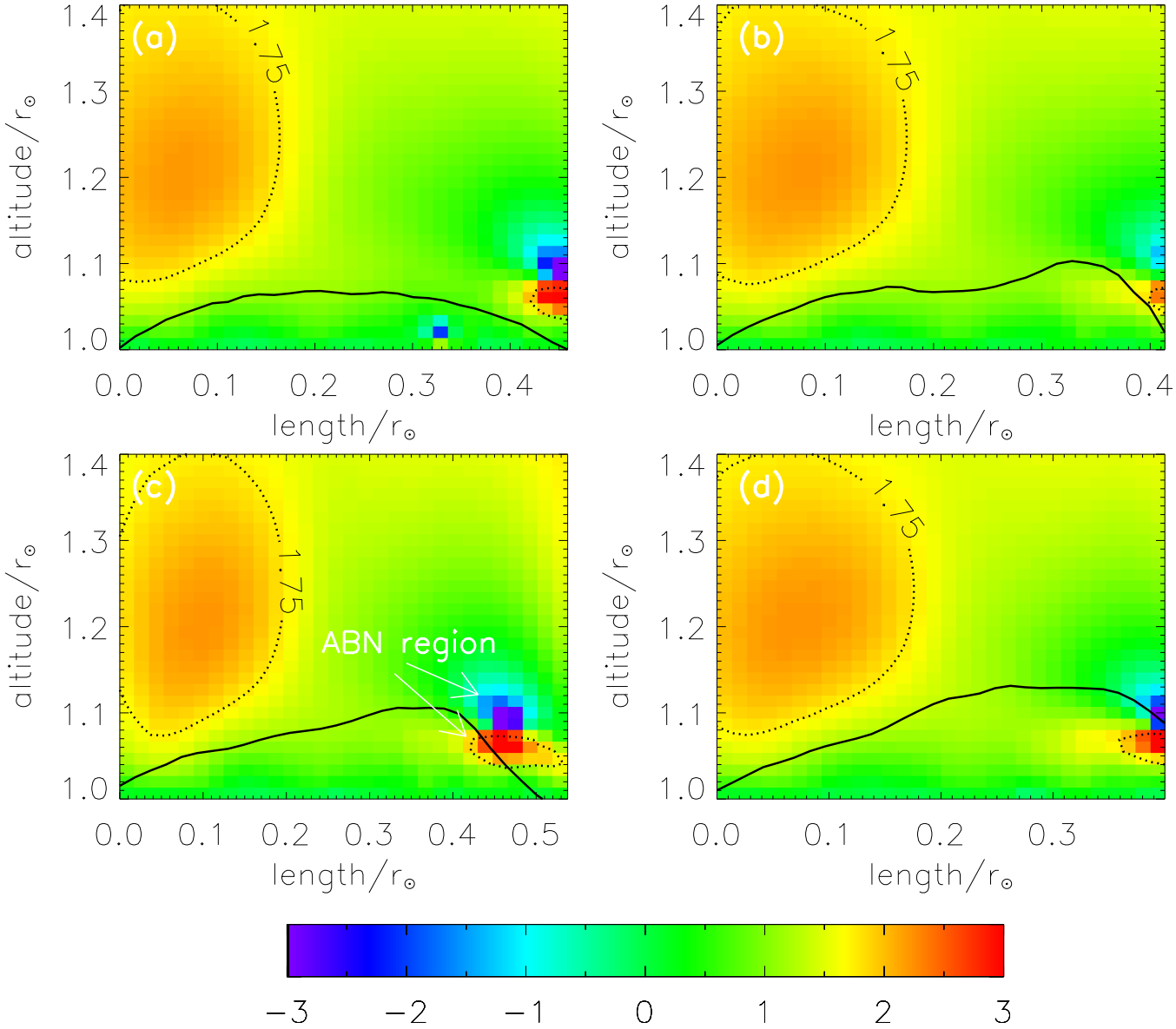

Figure 4. The distribution of decay index n on the radial slice over F1, at 13:06, 13:26, 13:46, and 14:06 UT. The black solid lines indicate the filament, which is plotted from its western foot to the eastern one over these four planes. The contour lines of decay index n are overplotted as dotted lines on every frame, and the contour value is 1.75. The ABN region is marked by white arrows in frame (c).

this question, the spatial distribution of n must be closely examined.

In this paper, we present a detailed study on the distribution of n for two asymmetrical eruptive events, in which particular ABN regions are first identified and precisely located near the filaments' split legs. The magnetic topological structures of the studied filaments have also been inspected and the results are shown in Figures 7 and 8. From the overlying magnetic topological images of F1 and F2, we can infer that the magnetic topological structures are very different in these ABN regions where the filament started to break. The magnetic connectivity varies strongly in these ABN regions and this configuration is also known as a magnetic quasi-separatrix layer (QSL; Titov 2002), in which a magnetic reconnection tends to occur preferentially (Aulanier 2010).

According to these observations, we interpret the spatial relationship of QSLs and ABN regions within the framework of the magnetic breakout model (Antiochos 1998; Antiochos et al. 1999). As the model proposed, a core filament is assumed to be surrounded by a quadrupolar loop system as shown in Figure 9. A special QSL is shown above the multipolar source region composed of two internal loop systems and a large overlying magnetic arch system. Because of the peculiar connectivity of this configuration, a V-shaped horizontal field profile can be expected between the two internal loop systems. When the slope of this V-shaped structure is steep enough, an ABN region will form in this layer. Both the split of filaments' active leg and the location of ABN regions imply that the torus instability can be exerted only by a small ABN region and this instability is also the likely triggering mechanism for the breakage of the

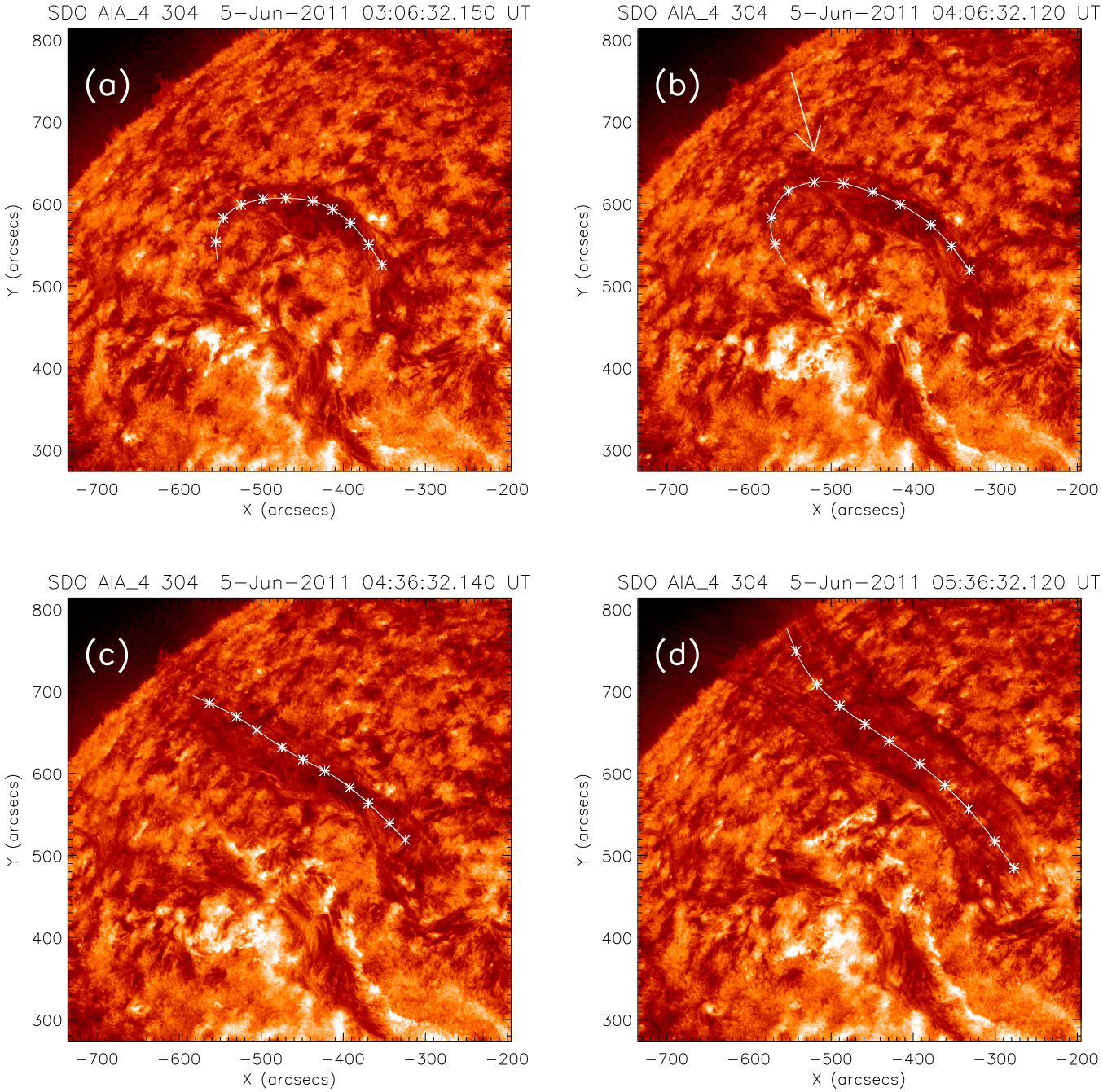

Figure 5. AIA observation of the eruption progress of F2. The white arrow in the frame (b) shows the location where the filament was broken. F2 is indicated by white asterisk lines.

filaments' body. We also stress that our interpretation is just a possible scenario for these two events presented here. We do not intend to exclude other possibilities for different asymmetric eruptions. Nevertheless, the structure of the overlying magnetic environment and the corresponding spatial distribution of the decay index n should be important for the study of filaments' stability and eruption.

In summary, the overlying magnetic field of asymmetric eruptive filaments is investigated in this paper and the results suggest a close relationship between the broken points of the filaments and the ABN regions of the decay index n corresponding to a special QSL. All of our analyses confirm the assumption of torus instability as a possible triggering mechanism for successful filament eruptions, as proposed by Kliem & Török (2006). In contrast to other investigations, we first focus on the spatial distribution of decay index n, and find that small ABN regions can really cause a local torus instability and result in an asymmetric eruption. On the other hand, this study also provides a possible way to forecast how a filament might erupt and predict the location where a partially eruptive filament could be broken. We further note that since all of our simple events are rope-like filaments, consistent with a flux

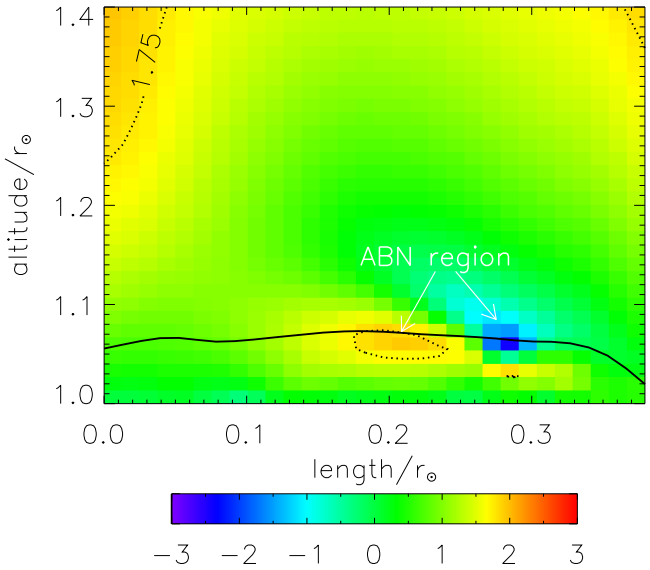

Figure 6. The n-map over F2 at 02:06 UT plotted in the curved plane along the filament, with the filament indicated by a black solid line. The n-map is plotted from the filament's western foot to its eastern foot. The ABN region and the contour of n at 1.75 are indicated by the white arrows and the black dotted lines, respectively.

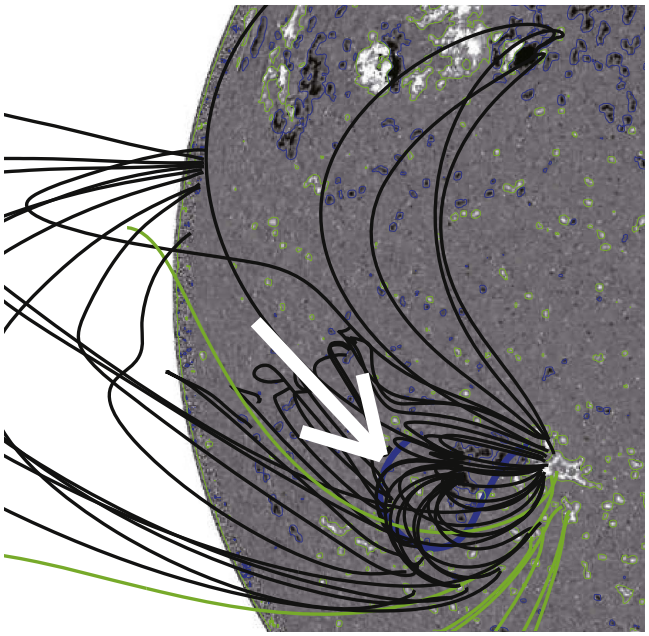

Figure 7. The magnetic environment of F1; the extrapolated three-dimensional coronal fields are overplotted on the *SDO*/HMI (Schou et al. 2012) magnetogram, in which the black (green) lines represent closed (open) field lines. The F1 is marked by a blue bold line and the white arrow indicates where the F1 erupted. The contour levels of the magnetogram are 10 G for positive polarities (green), and −10 G for negative polarities (blue).

rope model in which the filament material is frozen in flux ropes, all our findings should only apply to this category of filaments. Finally, we mention here that this work is just a tentative study on the peculiarities within the spatial distribution of the decay index n. Further theoretical and observational investigations are necessary, and encouraged, for better scrutinizing the relationship between the n index distribution and the filament eruption.

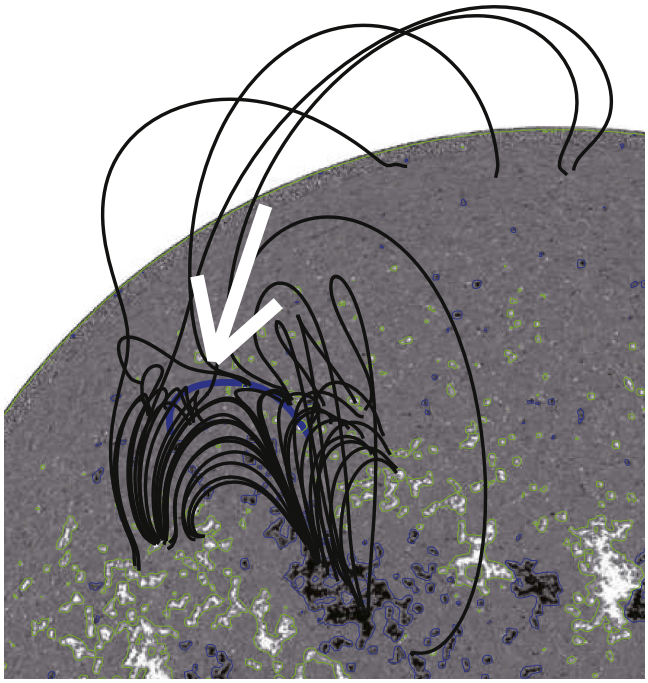

Figure 8. The magnetic environment of F2; the extrapolated three-dimensional coronal fields are overplotted as black solid lines on the *SDO*/HMI magnetogram, in which the blue bold line indicates F2 and its fractured location is indicated by the white arrow. The contours represent the magnetic field polarities at 10 G (green), and −10 G (blue).

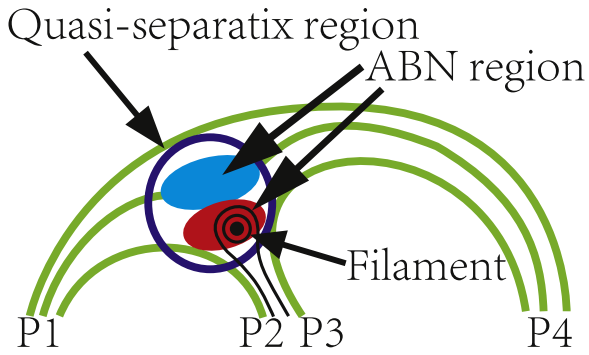

Figure 9. The schematic of a quasi-separatrix layer, in which P1–P4 indicate the four different magnetic poles, with P1 and P3 having the same polarity, which is opposite to that of P2 and P4. The magnetic separatrix region is marked by a blue circle, in which the ABN region is plotted as two colored (blue and red) ellipses.

The authors thank the anonymous referees for their valuable suggestions and comments, which significantly improved the work. The authors are also grateful to the *SDO*, *STEREO*, and *SOHO* teams for their data and corresponding analysis software. This work is supported by Grants from National Scientific Foundation of China (NSFC 11073050, 11533009), and from the Key Laboratory of Geospace Environment, CAS, University of Science & Technology of China. Y.L. is partly supported by the Visiting Professor Programme of King Saud University. A.E. is supported by the Chinese Academy of Sciences Fellowships for young international scientists under grant 2012Y1JA0002.

REFERENCES

Antiochos, S. K. 1998, ApJL, 502, L181
Antiochos, S. K., DeVore, C. R., & Klimchuk, J. A. 1999, ApJ, 510, 485
Aulanier, G. 2010, Proceedings of the International Astronomical Union, 6, 233 (S273)
Bateman, G. 1978, MHD Instabilities (Cambridge, MA: MIT Press)
Fan, Y., & Gibson, S. E. 2007, ApJ, 668, 1232
Filippov, B. P., Martsenyuk, O. V., Den, O. E., et al. 2014, ARep, 58, 928
Forbes, T. 2000, in Encyclopedia of Astronomy and Astrophysics, ed. P. Murdin (Bristol: IOP Publishing), 2295
Hudson, H. S., Bougeret, J., & Burkepile, J. 2006, SSRv, 123, 13
Kaiser, M. L., Kucera, T. A., Davila, J. M., et al. 2008, SSRv, 136, 5
Kliem, B., & Török, T. 2006, PhRvL, 96, 255002
Lemen, J. R., Title, A. M., Akin, D. J., et al. 2012, SoPh, 275, 17
Lin, J., & Forbes, T. G. 2000, JGR, 105, 2375
Liu, R., Alexander, D., & Gilbert, H. R. 2009a, ApJ, 691, 1079
Liu, Y. 2008, ApJL, 679, L151
Liu, Y., Su, J., Xu, Z., et al. 2009b, ApJL, 696, L70
Low, B. C. 1996, SoPh, 167, 217
Parenti, S. 2014, LRSP, 11, 1
Pesnell, W. D., Thompson, B. J., & Chamberlin, P. C. 2012, SoPh, 275, 3
Priest, E. R., & Forbes, T. G. 2002, A&ARv, 10, 313
Scherrer, P., Bogart, R. S., Bush, R. I., et al. 1995, SoPh, 162, 129
Schou, J., Borrero, J. M., Norton, A. A., et al. 2012, SoPh, 275, 327
Schrijver, C. J., & De Rosa, M. L. 2003, SoPh, 212, 165
Titov, V. S. 2002, JGR, 107, 1164
Török, T., & Kliem, B. 2005, ApJL, 630, L97
Tripathi, D., Isobe, H., & Mason, H. E. 2006, A&A, 435, 1111
Wuelser, J.-P., Lemen, J. R., Tarbell, T. D., et al. 2004, Proc. SPIE, 5171, 111
Zhang, H. 2002, MNRAS, 332, 500
Zuccarello, F. P., Seaton, D. B., Mierla, M., et al. 2014, ApJ, 785, 88